PAPER

Check for updates

Al–Pt compounds catalyzing the oxygen evolution reaction†

Ana María Barrios Jiménez,[a] Olga Sichevych, [ID][a] Ioannis Spanos, [ID][b] Simone G. Altendorf, [ID][a] Alim Ormeci [ID][a] and Iryna Antonyshyn [ID] *[a,c]

Al–Pt compounds have been systematically studied as electrocatalysts for the oxygen evolution reaction (OER). Considering the harsh oxidative conditions of the OER, all Al–Pt compounds undergo modifications during electrochemical experiments. However, the degree of changes strongly depends on the composition and crystal structure of a compound. In contrast to Al-rich compounds (Al_4Pt and $Al_{21}Pt_8$), which reveal strong leaching of aluminum, changes in other compounds (Al_2Pt, Al_3Pt_2, rt-AlPt, Al_3Pt_5, and rt-$AlPt_3$) take place only on the surface or in the near-surface region. Furthermore, surface modification leads to a change in the electronic structure of Pt, giving rise to the *in situ* formation of catalytically more active surfaces, which are composed of intermetallic compounds, Pt-rich Al_xPt_{1-x} phases and Pt oxides. Forming a compromise between sufficient OER activity and stability, Al_2Pt and Al_3Pt_2 can be considered as precursors for OER electrocatalysts.

Introduction

Activity is a crucial feature of an electrocatalyst in the oxygen evolution reaction (OER), but its stability under the oxidative conditions of the OER in acidic media also plays an important role.[1,2] Therefore, mainly noble metal-based catalysts are considered for the anode reaction in proton exchange membrane (PEM) electrolyzers.[1,3,4] Due to the limited resources of noble metals and, as a result, their high costs, many research groups are looking for materials with reduced amounts of noble metals or their complete substitution.[5]

Platinum is one of the most stable noble metals against dissolution.[2a,6] Hence, one attractive approach to develop active and stable OER electrocatalysts is to increase the inherent activity of Pt while profiting from its excellent stability. This can be realized through the formation of intermetallic compounds,[7] as the modification of the electronic states of Pt together with the change in its atomic environment on the catalyst surface will lead to different adsorption properties and, correspondingly, to a different OER electrocatalytic performance.

The formation of intermetallic compounds (*e.g.* combining Pt with Al) allows modifying the electronic state of an active component and at the same time tailoring material stability. On one hand, the bonding in Al–Pt intermetallic compounds with essential ionic contribution[8] is expected to increase the chemical stability of these materials against dissolution under the harsh OER conditions. Moreover, the pronounced charge transfer from aluminum to platinum for all Al–Pt compounds[8] makes the Pt atoms in the Al–Pt compounds not equivalent to those in elemental Pt, which should modify the OER overpotential of the resultant materials while maintaining the desired stability.

On the other hand, aluminum as one of the Earth's most abundant metals,[9,10] is widely used in alloys for industrial purposes, considering its low cost, non-toxicity, high electrical conductivity, adequate mechanical strength, low specific gravity and good resistance to corrosion,[9,11] making it an excellent candidate to be used as a counterpart element in catalytic materials.

Experimental

Al–Pt compounds (Al_4Pt, $Al_{21}Pt_8$, Al_2Pt, Al_3Pt_2, rt-AlPt, Al_3Pt_5 and rt-$AlPt_3$) were synthesized by arc melting of the initial components (Pt granules (Chempur, 99.99%) and Al rods (Alfa Aesar, 99.9965%)) in corresponding atomic ratios. The samples were turned over and re-melted three times to ensure homogeneity. The obtained ingots were placed in alumina crucibles, sealed under argon in Ta containers and afterwards - in

[a]Max-Planck-Institut für Chemische Physik fester Stoffe, Nöthnitzer Str. 40, 01187 Dresden, Germany. E-mail: Antonyshyn@fhi-berlin.mpg.de
[b]Max-Planck-Institut für Chemische Energiekonversion, Stiftstraße 34-36, 45470 Mülheim an der Ruhr, Germany
[c]Fritz-Haber-Institut der Max-Planck-Gesellschaft, Faradayweg 4-6, 14195 Berlin, Germany

evacuated quartz tubes. Homogenization annealing was performed according to the phase diagram of the Al–Pt system.[12] The temperature was controlled with a thermocouple before the samples were introduced into a pre-heated oven. After the heat treatment, the samples were quenched by breaking the quartz ampoules in cold water. The information about the annealing temperatures and the dwelling time for various Al–Pt compounds is given in Table S1.†

In order to shape the specimens for electrochemical experiments, the annealed ingots were ground in an agate mortar and transferred into a carbon press die (8 mm in diameter). Densification was carried out *via* spark plasma sintering (SPS), heating up at the rate of 100 K min^{-1} to a corresponding temperature (T_{max}) and holding it for a certain time (t) at constant pressure (P) (Table S2†). Afterwards, the samples were cooled down by switching off the heating. The density of all densified Al–Pt samples was above 95%.

After SPS, the cylinders were initially polished manually with a SiC grinding paper (Grit 100, 400, 500), and afterwards rotating the plate with SiC grinding papers (Grit 800, 1200, 2400 and 4000) on a grinding machine (LaboPol-21) at 250 rpm. Further polishing to a mirror surface was performed with diamond solutions (diamond particle size 3, 1, and $\frac{1}{4}$ μm in diameter) and a water-based green lubricant from Struers on a rotating MD Dur plate at 800 rpm using a polishing machine (RotoPol-15). The polishing procedure was carried out before each electrochemical experiment.

To characterize the synthesized samples, powder X-ray diffraction (PXRD) was applied. The pieces of the synthesized ingots were ground in an agate mortar and put between two Kapton foils onto a special PXRD holder. The X-ray powder diffraction patterns were measured in the transmission geometry with a Huber Imaging Plate Guinier Camera G670 (Cu Kα$_1$, λ = 1.54056 Å). A phase analysis was performed by comparing the experimental patterns with the calculated ones using the program WinXPOW.[13]

To study the chemical state of the electrochemically treated samples, laboratory X-ray photoelectron spectroscopy (XPS) was performed. The experiments were done at room temperature using a Vacuum Generators twin crystal monochromatized Al-Kα ($h\nu$ = 1486.6 eV) source and a Scienta R3000 electron energy analyzer in normal emission geometry. The overall energy resolution was set to about 0.4 eV and the Fermi level was calibrated using a polycrystalline Ag reference. The pressure in the spectrometer chamber was in the 10^{-10} mbar range. The data analysis was done by comparing the experimental XPS spectra (mainly the positions of the peaks) with those available in the literature.

The electrochemical experiments were performed in a three-compartment electrochemical cell using a Bio-Logic SP-300 potentiostat. A Pt wire (PINE, 99.99%, 0.5 mm in diameter) and a saturated calomel electrode (PINE, Hg/Hg$_2$Cl$_2$, 4 M KCl) were used as the counter and reference electrodes, respectively. The cylinders of the Al–Pt specimens were inserted as working electrodes in the electrochemical cell. The measurements were carried out in Ar-saturated 0.1 M HClO$_4$

(prepared by dilution of 70% HClO$_4$ (Aldrich, 99.999% trace metal basis) in Millipore water with a resistivity of 18.2 MΩ cm). Purging with argon (purity grade 5.0) was done for 30 min prior to each experiment in order to de-aerate the electrolyte. Initially, the cyclic voltammetry (CV) technique was performed up to the maximum potential (E_{max}) of 1.0 V$_{RHE}$ (sweep rate of 50 mV s^{-1}; 50 cycles). To estimate the OER activity of the studied Al–Pt compounds, the linear sweep voltammetry (LSV) technique was employed (E_{max} = 2.0 V$_{RHE}$; sweep rate of 5 mV s^{-1}). To monitor the change in the OER activity over time, the chronopotentiometry (CP) technique was applied at the benchmark current density of 10 mA cm^{-2} for 2 h.[3c,14] To check the OER activity of the sample during the CP measurement, LSVs were additionally recorded after 1 h and 2 h of CP. In order to release the system, an open circuit voltage (OCV) measurement was performed for 5 min before each LSV. The current densities (j) were normalized to the geometrical area of the Al–Pt cylinders (0.204 cm^2). All values of the potentials were IR-corrected (at 85%) and expressed *versus* a reference hydrogen electrode (RHE). The EC-Lab software was used for controlling the electrochemical experiments and also for recording and processing the obtained results.[15]

The concentrations of the dissolved elements (Al and Pt) were determined by taking electrolyte aliquots at the end of each EC experiment. Two electrolyte probes after each electrochemical experiment were analyzed *via* inductively coupled plasma-optical emission spectrometry (ICP-OES 5100 SVDV, Agilent). The aliquots were handled without dilution since the obtained concentrations did not exceed the maximum value of the linear calibration. The calibration was performed using a six-point standard calibration series and a blank probe of 0.1 M HClO$_4$.

The all-electron full-potential local orbital FPLO method[16] was employed to calculate the electronic density of states (DOS) for Pt. The local density approximation to the density functional theory as parametrized by Perdew and Wang[17] was used to account for the exchange–correlation effects. The fully-relativistic calculations[18,19] were performed for the experimentally determined crystal structure data. The DOS projected on the orbitals occupied according to the free atom electronic configurations were weighted by the photoionization cross sections[20] and broadened by a Gaussian function of width 0.4 eV.

Results and discussion

The Al–Pt intermetallic compounds present a variety of crystal structures and can be grouped as follows: (i) the crystal structures of the Al-rich compounds (Al$_4$Pt[21] and Al$_{21}$Pt$_8$[21a,22,23a]) represent their own structural patterns based on the (defect) icosahedral environment of Pt atoms surrounded by Al atoms; (ii) the compounds in the middle part of the Al–Pt system (Al$_2$Pt,[21a,23] Al$_3$Pt$_2$,[23a,24] and rt-AlPt[23b,24b,25]) are described as the derivatives of the close packing of atoms with Pt atoms, surrounded by Al in the form of (distorted) cubes; and (iii) the Pt-rich phases (Al$_3$Pt$_5$[23b,26] and rt-AlPt$_3$[24a,26a,27]) are derivatives
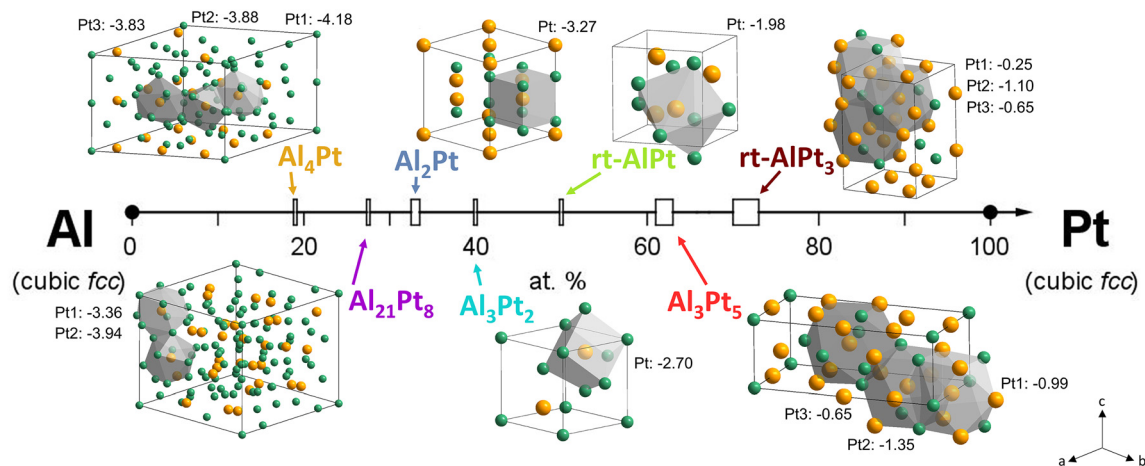
Fig. 1 Intermetallic Al–Pt compounds and their crystal structures (Pt atoms are in orange and Al in green). The coordination polyhedra are presented for the Pt1, Pt2 and Pt3 atoms. The QTAIM charges of the Pt atoms in the Al–Pt compounds are added from ref. 8.

of the closest packing, similar to elemental Pt (Fig. 1). The Pt QTAIM charges, obtained from the Quantum Theory of Atoms in Molecules approach, in the Al–Pt compounds decrease with increasing Al content, starting from zero in elemental Pt (Fig. 1 and S1†).[8] Only high-temperature (ht) modification of AlPt was considered in ref. 8. Thus, the charge distribution between Al and Pt for the room-temperature (rt) modification was calculated in the present work. Different scenarios of the atomic interactions in Al–Pt compounds as a result of the various crystal structures lead to the different electronic states of Al and Pt. Changes in the electronic state of the Pt atoms in Al–Pt compounds are also confirmed by spectroscopic studies *via* hard X-ray photoelectron spectroscopy (HAXPES).[28] The shift of the Pt 4f core level towards higher binding energies (BE) with decreasing Pt content was explained by the charge transfer from Al to Pt in Al–Pt compounds.

The powder X-ray diffraction (PXRD) patterns of the synthesized compounds confirm the phase purity of most of the Al–Pt compounds (Fig. 2). Only the PXRD patterns of Al_3Pt_2 and rt-AlPt specimens reveal traces of rt-AlPt and ht-AlPt, respectively. However, the contributions of the secondary phases were negligible and the samples were used for further electrochemical experiments. The lattice parameters of the studied Al–Pt compounds (Table S3†) are comparable with those published in the literature.[21–27]

The characterized Al–Pt samples were ground and densified into cylinder-shaped specimens (*cf.* Experimental), which were used as working electrodes for the electrochemical experiments to assess their OER activity.

The results of the linear sweep voltammetry (LSV) of the Al-rich compounds Al_4Pt and $Al_{21}Pt_8$ stand out within the Al–Pt compounds due to their high current density values at potentials below the theoretical OER onset potential (1.23 V_{RHE}) (Fig. 3). This points out the predominance of the other processes, such as dissolution, occurring at the surface of these materials at the applied anodic potentials. Considering the chemical properties of aluminum, its high content in these
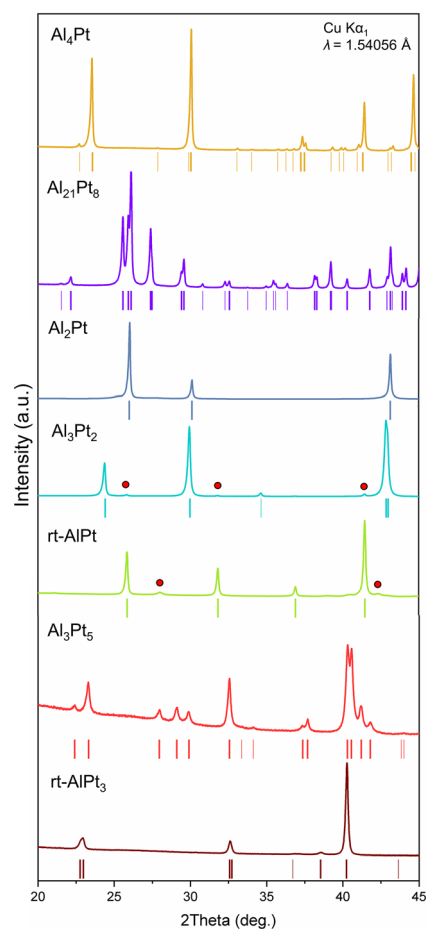

Fig. 2 PXRD patterns of the prepared Al–Pt compounds. The peak positions of the calculated patterns are shown below the corresponding experimental patterns with colored ticks. The reflections of the secondary phases are marked by red circles.
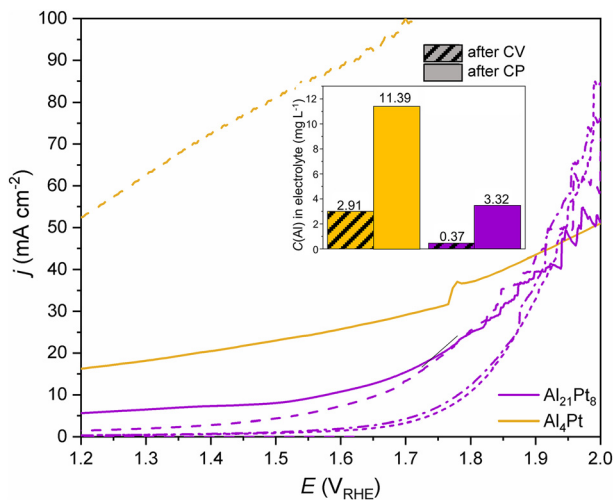
Fig. 3 LSVs with Al-rich compounds as anode materials: initial (solid lines), after the CV pre-treatment (dashed lines), after one hour of CP (dash-dot lines), and after two hours of CP (short-dash lines). Inset: Concentration of Al in the electrolyte (in mg L^{-1}) after the CV and CP experiments.

compounds and the Pourboix diagrams,[29] the dissolution of aluminum in acidic solutions at the applied potentials should be considered. Therefore, the activity of Al_4Pt and $Al_{21}Pt_8$ as OER electrocatalysts was not compared with other Al–Pt compounds, since the overpotential values at a current density of 10 mA cm^{-2} (η_{10}), obtained from the LSV data, are predominantly influenced by the dissolution processes. Furthermore, it is complicated to distinguish the on-going Al dissolution and the beginning of the oxygen evolution reaction. These suggestions have experimental confirmation. After the cyclic voltammetry (CV) pre-treatment of Al_4Pt (Fig. S2†), the values of current density above 50 mA cm^{-2} were obtained at potentials below the theoretically calculated onset of the OER reaction (1.23 V$_{RHE}$, Fig. 3). From the presence of Al in the electrolyte (inset of Fig. 3), the pronounced dissolution of Al from Al_4Pt at anodic potentials lower than 1.23 V$_{RHE}$ can be concluded. In this case, chronopotentiometry (CP) was performed for less than 200 s due to the visual instability of the sample in the electrolyte. The curiously low potential values obtained by passing through the sample a current density of 10 mA cm^{-2} show the dominance of the dissolution process and no OER (Fig. S3†).

In the case of $Al_{21}Pt_8$, the CV pre-treatment leads to a less-pronounced Al dissolution (compared to the Al-richest compound Al_4Pt) and the contribution of the dissolution process to the LSV is suppressed in this case (Fig. 3). Despite the partial Al dissolution during the CP experiment (inset of Fig. 3), LSVs after one and two hours of CP are comparable and it becomes possible to differentiate η_{10} values from these data. This means that passing constant current through the sample allows achieving the nearly steady state at the surface of $Al_{21}Pt_8$. The almost constant potential, measured during the second hour of the CP experiment (Fig. S4†), confirms this fact and agrees with the LSV data measured afterwards.

The summary of the OER activity, represented as η_{10} values, for other Al–Pt binary intermetallic compounds is shown in Fig. 4a. The experimental LSVs are shown in Fig. S5.† After the CV pre-treatment (Fig. S2†), a clear activation of the compounds was observed: the η_{10} values are 60–100 mV lower (30 mV for elemental Pt) compared to that obtained from the initial LSVs. This reduction in the OER overpotentials after CV evidences changes on the surfaces of the Al–Pt compounds, creating a catalytically more active surface for the OER. However, within the Al–Pt system, no clear correlation between the OER activity and composition was found.

Looking at the results of CP experiments (Fig. 4b), for Al_2Pt the initial drop in potential by 100 mV during the first hour of CP followed by the stabilization of the measured potential during the second hour of the CP, indicate an initial activation (changes) of the material, which is followed by approaching a nearly steady state after two hours of CP. There is also a moderate amount of 0.23 mg L^{-1} of Al in the electrolyte after the CP for Al_2Pt. The promising performance of this compound towards the OER has already been reported.[30] The compound
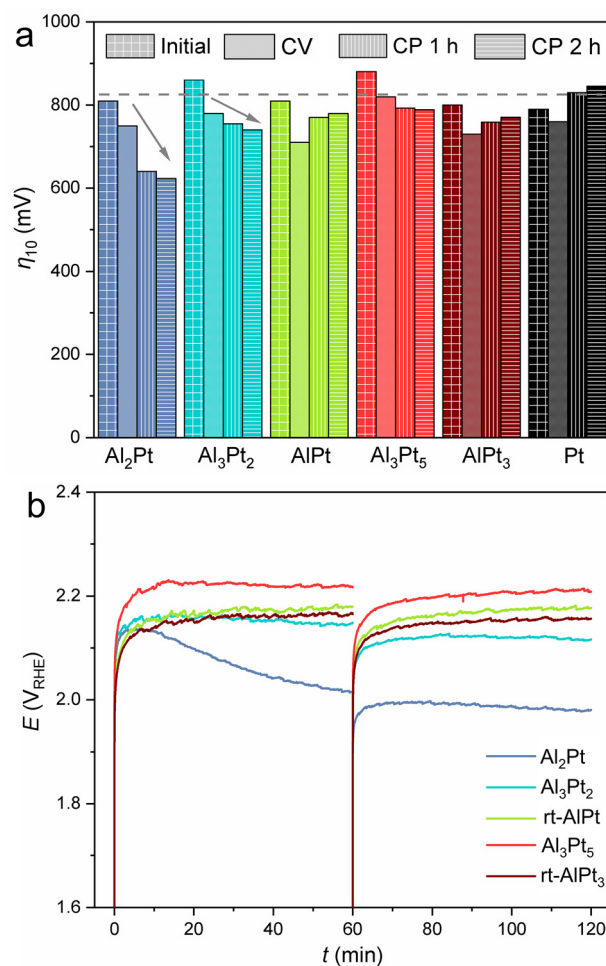

Fig. 4 (a) η_{10} values for the Al–Pt compounds after different electrochemical experiments and (b) the CP results for the selected Al–Pt compounds at j = 10 mA cm^{-2} for 2 h.

Al_3Pt_2 also shows activation during the CP experiment, however, not so pronounced as Al_2Pt. Other Al–Pt compounds (rt-AlPt, Al_3Pt_5 rt-AlPt$_3$) and elemental Pt do not show significant differences in OER activity after the 1st and 2nd hours of CP. The amounts of dissolved Al in these cases are either negligible or below the detection limit of ICP-OES (Table S4†).

Compared to elemental Pt, the Al–Pt electrode materials possess reduced OER overpotentials. Furthermore, the η_{10} values are comparable with those of other noble metals that are *a priori* more active than Pt, such as Rh (*ca.* 600 mV) and Pd (*ca.* 670 mV).[2a] The comparison with other earth-abundant electrocatalysts is hampered by their different scales and shapes (nanoparticles, core–shell, *etc.*). Among the bulk intermetallic compounds, the OER activity was studied *e.g.*, for the isostructural compounds Fe_2Ta (770 mV), Co_2Ta (600 mV) and Ni_2Ta (570 mV) in an acidic electrolyte.[31] The OER activity of the studied Al–Pt compounds is close to those ones.

To shed light onto the surface changes of the selected Al–Pt compounds ($Al_{21}Pt_8$, Al_2Pt and Al_3Pt_2), the electronic state of the Pt atoms was investigated *via* X-ray photoelectron spectroscopy (XPS, Fig. 5). The XPS results for compound Al_4Pt are presented separately (Fig. S6†), since the duration of the CP experiment differs from that of the other Al–Pt compounds. In contrast to the HAXPES spectra of the as-synthesized Al–Pt compounds[28] with single contributions from the intermetallic compounds (the corresponding positions of the Pt 4f core levels are presented in Table S5†), those after two hours of CP are composed of multiple contributions (Fig. 5). The Pt 4f core levels identified for the intermetallic compounds are shifted towards lower binding energies and closer to elemental Pt (70.9 and 74.2 eV for Pt $4f_{7/2}$ and $4f_{5/2}$, respectively),[28] and their values are summarized in Table 1. These shifts of the Pt 4f core levels evidence that the electronic structures of the resultant materials are different from the initial ones.[28]

Fig. 5 Normalized XPS spectra of the Pt 4f core levels for the selected Al–Pt compounds after 2 h of CP.

Table 1 The Pt $4f_{7/2}$ XPS core level and its shift with respect to elemental Pt for the selected Al–Pt compounds after two hours of CP

Compound	Pt $4f_{7/2}$ BE, eV	Shift, eV
Pt	70.9	—
Al_3Pt_2	71.31	0.41
Al_2Pt	71.13	0.23
$Al_{21}Pt_8$	71.13	0.23
Al_4Pt	71.12	0.22

Interestingly, the positions of the Pt 4f core levels follow the opposite trend as in the initial materials. The Pt 4f core levels of Al_4Pt, $Al_{21}Pt_8$, Al_2Pt and Al_3Pt_2 are closer to the values obtained for elemental Pt (70.9 and 74.2 eV for Pt $4f_{7/2}$ and $4f_{5/2}$, respectively) and the shift in binding energy with respect to the initial position is larger for those compounds. Probably, this is related to the different dissolution rates of Al, which are evidenced by the presence of Al in the electrolytes in the case of Al-rich compounds. Therefore, Pt is losing the electrons that Al is contributing and the Pt 4f core level shifts towards lower binding energies, probably due to the emptier Pt valence 5d states. Since adsorption is mediated by d valence electrons,[32] this could explain the better activity of Al-rich compounds: the modifications on the surface are stronger for those compounds, giving rise to emptier 5d valence states and facilitating electron transfer from the adsorbates.

The XPS signals at the binding energies 74.45 and 77.3 eV are assigned to PtO_2 (from the literature: 74.5 and 77.7 eV for Pt $4f_{7/2}$ and $4f_{5/2}$, respectively[33]). The oxide PtO_2 is formed on the surfaces of Al_3Pt_2, Al_2Pt and $Al_{21}Pt_8$. In addition, two signals are identified at 72.4 and 75.7 eV and they are attributed to PtO (72.5 and 75.6 eV for Pt $4f_{7/2}$ and $4f_{5/2}$, respectively[33]), which indicate that PtO was initially formed on those surfaces and further oxidized to PtO_2 due to the harsh oxidative conditions at the applied anodic potentials without cathodic backward scans.

The formation of the Pt oxides does not hinder the OER activity of the compounds, since they do not cover completely the freshly formed OER-active Pt-rich phase (presumably solid solution Al_xPt_{1-x}[30]). This is obvious from the multiple contributions to the XPS signals. Furthermore, the steady state of the surface was not reached yet (LSV after one and two hours of CP are slightly different). Even if the modification of the surface is less pronounced than at the beginning, there are still ongoing changes on the surfaces (*e.g.*, Al dissolution) and, therefore, the new catalytically active phase is being continuously formed.

The XPS spectra of the Al 2s and O 1s core levels were also studied (Fig. S7†). However, the Al 2s core levels are not well-resolved for $Al_{21}Pt_8$, Al_2Pt and Al_3Pt_2 due to the reduced amount of Al on the surface and the small cross-section of this Al 2s orbital.[34] These facts together with the observed shifts in the Pt 4f core levels support the partial dissolution of Al into the electrolyte and the ICP-OES results. The O 1s core levels are quite broad and consist of many contributions: Pt–O (529.6 eV),[33] PtO (530.4 eV),[33] PtO_2 (531.1 eV),[36] hydrated O:
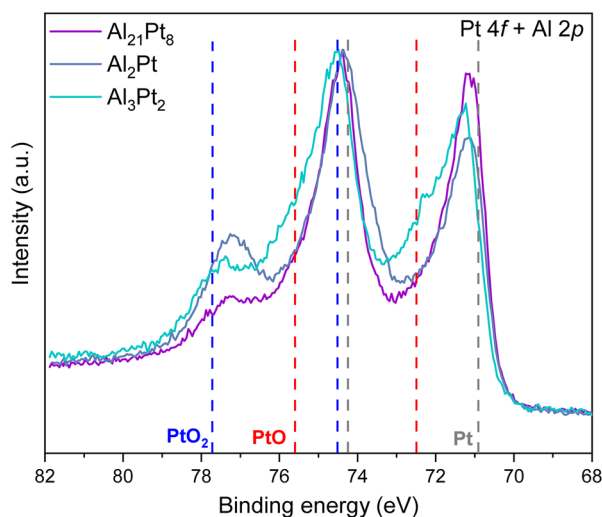
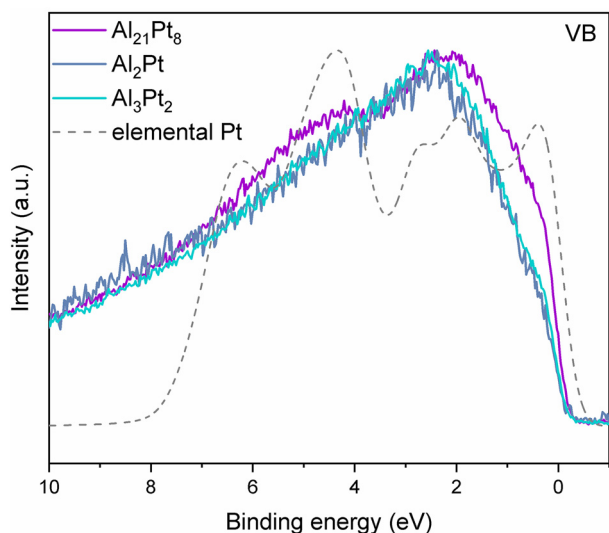**Fig. 6** Normalized XPS spectra of the valence bands for $Al_{21}Pt_8$, Al_2Pt and Al_3Pt_2 after 2 h of CP. The grey dashed line represents the calculated sum of the partial DOS for Pt, weighted by photoionization cross-section and broadened by a Gaussian of a full width at half maximum equal to 0.4 eV.

H_2O complexes (532.2 eV),[33] chemisorbed water (533 eV),[33] and α-Al_2O_3 (530.7 eV).[35] These contributions are in good agreement with those obtained upon the anodization of elemental Pt using NAP-XPS.[33] Pt oxides and α-Al_2O_3 are the main contributors in the case of Al_3Pt_2, whereas $Al_{21}Pt_8$ and Al_2Pt are oxidized even more strongly with the appearance of the O:H_2O complexes and chemisorbed water on the surface. This fact proves the observation made for the Pt 4f core levels: PtO is initially formed on the surfaces and is oxidized further to PtO_2 during the course of the OER experiment.

The valence band features of the studied Al–Pt compounds after the electrochemical experiments resemble the weighted DOS of elemental Pt, proving the formation of the Al_xPt_{1-x} phase after the electrochemical experiments (Fig. 6). Hence, the binary compounds Al_2Pt and Al_3Pt_2 act as OER catalyst precursors. Surface transformations take place during the course of the reaction as Al partially leaves the material. In this transition state, Pt is undercoordinated and more prone to take electrons from the surroundings, adsorbing the OH species easier. This leads to the activation of the material. Then, the Pt atoms at the surface take up new electronic and geometrical features to optimize their bonding configurations, giving rise to a new freshly formed Al_xPt_{1-x} phase, leading to the nearly steady state of the materials. This Al_xPt_{1-x} phase acts as a new OER electrocatalyst, which is more active than the intermetallic precursors.

Conclusions

The intermetallic Al–Pt compounds were investigated as OER electrocatalysts. A reliable comparison of the OER activity of the different Al–Pt compounds requires the treatment of the surface (*e.g.* CV, CP), aiming to reach a steady state. At the near-steady state, the Al–Pt compounds exhibit improved OER activity compared to elemental Pt and the trend becomes clear: a better OER activity in the case of the intermetallic compounds $Al_{21}Pt_8$, Al_2Pt and Al_3Pt_2. However, due to the surface modifications under the OER conditions, the OER activity of these compounds cannot be directly related to either the initial charges of the Pt atoms or any geometric features. At the same time, the influence of the surface morphological features on the OER catalytic performance cannot be excluded. The surface changes of the studied Al–Pt compounds are clearly evidenced by XPS measurements:

(i) Pt atoms have a different electronic state after the electrochemical experiments as the binding energies are shifted towards lower values (compared to pristine intermetallic compounds). The state is closer to Pt^0 as it loses the electrons contributed by the counterpart element Al. The emptier 5d states of Pt are more suitable for electron transfer and easier adsorption of the OH species.

(ii) The initial trend of the Pt 4f binding energies with composition is inverted to that after electrochemical treatment. In Al-richer compounds, more Al leaves the structure, modifying to a larger extent their structural and electronic properties.

(iii) Pt oxides are present on the surface after the CP experiment, due to the oxidative conditions at the applied anodic potentials. However, the Pt oxide formation is not sufficient to obstruct the good OER performance of the *in situ*-formed Al_xPt_{1-x} phase.

These results shed light on the electrochemical behaviour of the Al–Pt compounds under the OER conditions. The compounds do not maintain their structural and electronic properties during the OER as Al leaches into the electrolyte, leading to surface reconstruction (and roughening) and the formation of an OER-active Al_xPt_{1-x} phase. The compounds Al_2Pt and Al_3Pt_2 can be considered as precursors for OER active electrocatalysts, revealing a compromise between electrocatalytic activity and stability under OER conditions.

Conflicts of interest

There are no conflicts to declare.

Acknowledgements

References

1 T. Reier, H. N. Nong, D. Teschner, R. Schlögl and P. Strasser, *Adv. Energy Mater.*, 2017, **7**, 1601275.

2 (*a*) S. Cherevko, A. R. Zeradjanin, A. A. Topalov, N. Kulyk, I. Katsounaros and K. J. J. Mayrhofer, *ChemCatChem*, 2014, **6**, 2219; (*b*) S. Cherevko, *Curr. Opin. Electrochem.*, 2018, **8**, 118; (*c*) C. Spöri, J. T. Hong Kwan, A. Bonakdarpour, D. P. Wilkinson and P. Strasser, *Angew. Chem., Int. Ed.*, 2017, **56**, 2; (*d*) F.-Y. Chen, Z.-Y. Wu, Z. Adler and H. Wang, *Joule*, 2021, **5**, 1; (*e*) J. Masa, C. Andronescu and W. Schuhmann, *Angew. Chem., Int. Ed.*, 2020, **59**, 15298.

3 (*a*) M. Carmo, D. L. Fritz, J. Mergel and D. Stolten, *Int. J. Hydrogen Energy*, 2013, **38**, 4901; (*b*) E. Fabbri, A. Habereder, K. Waltar, R. Kötz and T. J. Schmidt, *Catal. Sci. Technol.*, 2014, **4**, 3800; (*c*) C. C. L. McCrory, S. Jung, I. M. Ferrer, S. M. Chatman, J. C. Peters and T. F. Jaramillo, *J. Am. Chem. Soc.*, 2015, **137**, 4347.

4 T. Reier, M. Oezaslan and P. Strasser, *ACS Catal.*, 2012, **2**, 1765.

5 (*a*) Y. Cheng and S. P. Jiang, *Prog. Nat. Sci.: Mater. Int.*, 2015, **25**, 545; (*b*) A. Li, Y. Sun, T. Yao and H. Han, *Chem. – Eur. J.*, 2018, **24**, 18334; (*c*) X. Zhao, W. Cheng, H. Zhang, W. Che, F. Tang and Q. Liu, *ACS Appl. Mater. Interfaces*, 2019, **11**, 34854; (*d*) J. Yan, J. Jin, M. Lu, B. Huang, H. Zhang, Y. Peng, P. Xi and C.-H. Yan, *J. Am. Chem. Soc.*, 2020, **142**, 18378.

6 S. Cherevko, *J. Electroanal. Chem.*, 2017, **787**, 11.

7 (*a*) M. Armbrüster, R. Schlögl and Yu. Grin, *Sci. Technol. Adv. Mater.*, 2014, **15**, 034803; (*b*) M. Armbrüster, *Sci. Technol. Adv. Mater.*, 2020, **21**, 303; (*c*) L. Rößner and M. Armbrüster, *ACS Catal.*, 2019, **9**, 2018; (*d*) S. Furukawa and T. Komatsu, *ACS Catal.*, 2017, **7**, 735; (*e*) C. Walter, P. W. Menezes and M. Driess, *Chem. Sci.*, 2021, **12**, 8603.

8 A. Baranov, M. Kohout, F. R. Wagner, Y. Grin and W. Bronger, *Z. Kristallogr.*, 2007, **222**, 527.

9 J. R. Davis, *ASM Specialty Handbook: Aluminum and Aluminum Alloys*, ASM International, Materials Park, Ohio, USA, 1993.

10 P. C. K. Vesborg and T. F. Jaramillo, *RSC Adv.*, 2012, **2**, 7933.

11 A. J. Downs, *Chemistry of aluminium, gallium, indium and thallium*, Blackie Academic and Professional, Chapman and Hall, London, UK, 1993.

12 A. J. McAlister and D. J. Kahan, in *Binary Alloy Phase Diagrams*, ed. T. B. Massalski, ASM International, Materials Park, Ohio, USA, 1990, pp. 195–197.

13 *WinXPOW (version 2.25)*, STOE and Cie GmbH, Darmstadt, Germany, 2009.

14 (*a*) C. C. L. McCrory, S. Jung, J. C. Peters and T. F. Jaramillo, *J. Am. Chem. Soc.*, 2013, **135**, 16977;

15 *EC-Lab software user's manual (version 11.30)*, BioLogic Science Instruments, Pariset, France, 2019.

16 K. Koepernik and H. Eschrig, *Phys. Rev. B: Condens. Matter Mater. Phys.*, 1999, **59**, 1743.

17 J. P. Perdew and J. Wang, *Phys. Rev. B: Condens. Matter Mater. Phys.*, 1992, **45**, 13244.

18 I. Opahle, K. Koepernik and H. Eschrig, *Phys. Rev. B: Condens. Matter Mater. Phys.*, 1999, **60**, 14035.

19 H. Eschrig, M. Richter and I. Opahle, in *Theoretical and Computational Chemistry*, ed. P. Schwerdtfeger, Elsevier, 2004, pp. 723–776.

20 J. J. Yeh and I. Lindau, *At. Data Nucl. Data Tables*, 1985, **32**, 1.

21 (*a*) B. Grushko and D. Kapush, *J. Alloys Compd.*, 2014, **594**, 127; (*b*) M. Wörle, F. Krumeich, T. Chatterji, S. Kek and R. Nesper, *J. Alloys Compd.*, 2008, **455**, 130.

22 (*a*) L.-E. Edshammar, *Acta Chem. Scand.*, 1966, **20**, 2683; (*b*) K.-J. Range and E. G. Christl, *J. Less-Common Met.*, 1988, **136**, 277.

23 (*a*) M. Ellner, U. Kattner and B. Predel, *J. Less-Common Met.*, 1982, **87**, 305; (*b*) R. Huch and W. Klemm, *Z. Anorg. Allg. Chem.*, 1964, **329**, 123; (*c*) E. Zintl, A. Harder and W. Haucke, *Z. Phys. Chem.*, 1937, **B35**, 354; (*d*) K. Chattopadhyay, S. Lele and P. Ramachandrarao, *J. Mater. Sci.*, 1978, **13**, 2730.

24 (*a*) T. Chattopadhyay and K. Schubert, *J. Less-Common Met.*, 1975, **41**, 19; (*b*) R. Ferro, R. Capelli and G. Rambaldi, *Atti Accad. Naz. Lincei, Cl. Sci. Fis., Mat. Nat., Rend.*, 1963, **34**, 45.

25 (*a*) K. Schubert, W. Burkhardt, P. Esslinger, E. Günzel, H. G. Meissner, W. Schütt, J. Wegst and M. Wilkens, *Naturwissenschaften*, 1956, **43**, 248; (*b*) P. Esslinger and K. Schubert, *Z. Metallkd.*, 1957, **48**, 126.

26 (*a*) M. Sauer, A. Engel and H. Lueken, *J. Alloys Compd.*, 1992, **183**, 281; (*b*) W. Klemm, F. Dorn and R. Huch, *Naturwissenschaften*, 1958, **45**, 490; (*c*) W. Bronger and K. Wrzesien, *J. Alloys Compd.*, 1996, **244**, 194.

27 (*a*) Y. Oya, Y. Mishima and T. Suzuki, *Z. Metallkd.*, 1987, **78**, 485; (*b*) W. Bronger, P. Müller and K. Wrzesien, *Z. Anorg. Allg. Chem.*, 1997, **623**, 362.

28 I. Antonyshyn, O. Sichevych, U. Burkhardt, A. M. Barrios Jiménez, D. Takegami, A. Melendez-Sans, Y.-F. Liao, K.-D. Tsuei, D. Kasinanthan and A. Ormeci, submitted.

29 M. Pourboix, *Atlas of electrochemical equilibria in aqueous solutions*, NACE International Cebelcor, Houston, Texas, USA, 1974.

30 I. Antonyshyn, A. M. Barrios Jiménez, O. Sichevych, U. Burkhardt, I. Veremchuk, M. Schmidt, A. Ormeci, I. Spanos, A. Tarasov, D. Teschner, G. Algara-Siller, R. Schlögl and Y. Grin, *Angew. Chem., Int. Ed.*, 2020, **59**, 16770.

31 J. S. Mondschein, K. Kumar, C. F. Holder, K. Seth, H. Kim and R. E. Schaak, *Inorg. Chem.*, 2018, **57**, 6010.

32 S. Furukawa and T. Komatsu, *ACS Catal.*, 2017, **7**, 735.

(*b*) I. Spanos, A. A. Auer, S. Neugebauer, X. Deng, H. Tüysüz and R. Schlögl, *ACS Catal.*, 2017, **7**, 3768.

33 R. Arrigo, M. Hävecker, M. E. Schuster, C. Ranjan, E. Stotz, A. Knop-Gericke and R. Schlögl, *Angew. Chem., Int. Ed.*, 2013, **52**, 11660.

34 (*a*) M. B. Trzhaskovskaya, V. I. Nefedov and V. G. Yarzhemsky, *At. Data Nucl. Data Tables*, 2001, **77**, 97;

(*b*) M. B. Trzhaskovskaya, V. K. Nikulin, V. I. Nefedov and V. G. Yarzhemsky, *At. Data Nucl. Data Tables*, 2006, **92**, 245.

35 J. A. Rotole and P. Sherwood, *Surf. Sci. Spectra*, 1998, **5**, 11.

36 M. Peuckert, F. P. Coenen and H. P. Bonzel, *Electrochim. Acta*, 1984, **29**, 1305.